molecular pharmaceutics

Article

111In and 225Ac-labeled cixutumumab for imaging and alpha particle radiotherapy of IGF-1R positive triple negative breast cancer

Viswas Raja Solomon, Elahe Alizadeh, Wendy Bernhard, Siddesh V. Hartimath, Wayne Hill, Rufael Chekol, Kris M Barreto, Clarence Ronald Geyer, and Humphrey Fonge

Mol. Pharmaceutics, **Just Accepted Manuscript** • DOI: 10.1021/acs.molpharmaceut.9b00542 • Publication Date (Web): 13 Sep 2019

^{111}In and ^{225}Ac-labeled cixutumumab for imaging and alpha particle radiotherapy of IGF-1R positive triple negative breast cancer

Viswas Raja Solomon[1], Elahe Alizadeh[1], Wendy Bernhard[2], Siddesh V. Hartimath[1], Wayne Hill[2], Rufael Chekol[1], Kris M. Barreto[2], Clarence Ronald Geyer[2*], Humphrey Fonge[1,3*]

[1]Department of Medical Imaging, University of Saskatchewan, College of Medicine, Saskatoon SK, Canada

[2]Department of Pathology and Laboratory Medicine, University of Saskatchewan, College of Medicine, Saskatoon SK, Canada

[3]Department of Medical Imaging, Royal University Hospital Saskatoon, Saskatoon SK, Canada

Authors for correspondence

*Humphrey Fonge, PhD

Email: humphrey.fonge@usask.ca

Tel: 306-655-3353

Fax: 306 655 1637

*Clarence Ronald Geyer, PhD

Email: ron.geyer@usask.ca

Tel: 306-966-2040

Abstract

Insulin growth factor receptor (IGF-1R) is overexpressed in many cancers of epithelial origin where it confers enhance proliferation and resistance to therapies targeted at other receptors. Anti-IGF-1R monoclonal antibodies have not demonstrated significant improvements in patient outcomes in clinical trials. Humanized monoclonal antibody cixutumumab (IMC-A12) binds to IGF-1R with low nM affinity. In this study cixutumumab was conjugated with *p*-SCN-Bn-DOTA and radiolabeled with ^{111}In or ^{225}Ac for imaging or radiotherapy using a triple negative breast cancer (TNBC) model SUM149PT. The antibody conjugate showed low nM affinity to IGF-1R which was not affected by conjugation and radiolabeling procedures. Cixutumumab immunoconjugates was effectively internalized in SUM149PT and was cytotoxic to the cells with an EC_{50} of ^{225}Ac-cixutumumab (0.02 nM) that was almost 5000-fold less than unlabeled cixutumumab (95.2 nM). MicroSPECT imaging of SUM149PT xenograft showed the highest tumor uptake occurred at 48 h post injection and was 9.9 ± 0.5 % injected activity per gram (%IA/cc). In radiotherapy studies, we evaluated the effect of specific activity of ^{225}Ac-cixutumumab on efficacy following a tail vein injection of two doses (day 0 and 10) of the investigation agent or controls. Cixutumumab (2.5 mg/kg) prolonged the survival of SUM149PT tumor bearing mice with a median survival of 87 days compared to PBS control group (median survival of 62 days). Median survival of high specific activity ^{225}Ac-cixutumumab (8 kBq/µg, 225 nCi, 0.05 mg/kg) was 103.5 days compared to 122 days for low specific activity ^{225}Ac-cixutumumab (0.15 kBq/µg, 225 nCi, 2.5 mg/kg). Additionally, low specific activity radioimmunoconjugate led to complete tumor remission in 2/6 mice. The data suggest that efficacy of cixutumumab can be enhanced by radiolabeling with ^{225}Ac at a low specific activity.

Keywords: Insulin Growth Factor Receptor type I (IGF-1R); Alpha Particle Radiotherapy; MicroSPECT Imaging; Triple Negative Breast Cancer; Cixutumumab

Introduction

Breast cancer is a leading cause of cancer-related deaths in women worldwide[1]. Among the several subtypes, 15–20% of diagnosed breast tumors are triple-negative breast cancer (TNBC) along with BRCA germline mutations[2, 3]. Recent preclinical and population studies demonstrated a role for insulin growth factor receptor (IGF-1R) signaling in TNBC. Amplification of IGF-1R is seen in residual disease following neoadjuvant chemotherapy in patients with TNBC, suggesting a potential contribution of IGF-1R signaling to chemotherapy resistance[4]. These findings demonstrate that IGF-1R signaling promotes tumor progression in TNBC and that IGF-1R signal inhibition may be a valuable target for TNBC imaging and radiotherapy. IGF-1R inhibition impeded the proliferation of TNBC cells with high IGF-1R expression *in vitro*[5, 6]. IGF-1R tyrosine kinase inhibitor (TKI) monotherapy was sufficient to reduce tumor size in a TNBC xenograft model[7, 8].

Several small-molecule inhibitors and antibodies directed against the IGF-1R have been developed and tested in phase I and II clinical trials[9-11]. Stable disease and objective response were reported in patients treated with these new agents, but no relationship with IGF-1R expression and response has been thoroughly investigated[10, 11]. Preclinical studies showed that IGF-1R expression is necessary for antitumor activity of anti–IGF-1R antibodies[12, 13]. Therefore, patient selection for IGF-1R–targeted therapy should be based on receptor expression. Thus far, studies on IGF-1R expression have been performed retrospectively on tumor tissue sections by immunohistochemistry (IHC). IHC cannot be used to measure IGF-1R expression in multiple lesions, especially in metastatic setting because of its invasive nature. Furthermore, the expression of IGF-1R may change over time.

The encouraging preclinical data seen with anti-IGF-1R antibodies have not been replicated in clinical trials. Clinical trials of anti-IGF-1R agents e.g. ganitumab, figitumumab, and cixutumumab have all not shown significant benefits in patients and most of these trials have been abandoned [14, 15]. The failure of anti-IGF-1R inhibitors means other approaches aimed at targeting this receptor could yield important benefits for patients. Our goal is to develop a theranostic pair using ^{111}In-labeled and alpha particle ^{225}Ac-labeled anti-IGF-1R antibody. The characteristics of ^{225}Ac: $t_{1/2}$ 10.0 days; energy range of 4 αs is 6 – 8 MeV (cumulative emission of 28 MeV/decay) decays with the emission of 5 αs, 3 β^- disintegrations, a range of 50 – 80 μm in tissues and with a linear energy transfer of up to 0.16 MeV/μm, makes this isotope ideal for radiotherapy, especially in micrometastatic settings. Recently, improved clinical outcomes have been obtained using alpha particle (e.g. ^{255}Ac and ^{213}Bi) labeled agents, particularly in prostate cancer and neuroendocrine tumors[16, 17].

Cixutumumab is a fully human IgG1/λ monoclonal antibody directed against IGF-1R. Cixutumumab binds IGF1R with high affinity and blocks interaction between IGF-1R and its ligands, IGF-1 and –2, and induces internalization and degradation of IGF-1R[18]. Anti-tumor effects of cixutumumab have been demonstrated in preclinical and clinical studies[18-20]. Currently, there are five ongoing clinical trials evaluating the efficacy of cixutumumab as either a single agent or in combination with other targeted therapies or chemotherapy agents[18-21]. For this purpose, we have used cixutumumab (IMC-A12) to develop a ^{111}In/^{225}Ac-cixutumumab theranostic agent against IGF-1R positive tumors. This is the first reported study of an anti-IGF-1R alpha particle radioimmunotherapeutic. Our hypothesis is that ^{225}Ac-cixutumumab will be more effective than cixutumumab in IGF-1R positive cells/tumor. ^{111}In-cixutumumab can be used for patient selection and for monitoring of response to anti-IGF-1R treatments as well as for dosimetry estimation for

^{225}Ac-cixutumumab radioimmunotherapy. We have evaluated the *in vitro* cytotoxicity and *in vivo* therapeutic potential in a mouse model with IGF-1R positive xenograft.

Materials and Methods

General

Chemicals used in the conjugation, radiolabeling, and purification steps were American Chemical Society reagent grade or better. Water and buffers were rendered metal-free by passing them through a column of Chelex-100 resin, 200–400 mesh (Bio-Rad Laboratories, Inc.), and were sterile-filtered through a 0.22 μm filter. The monoclonal antibody cixutumumab was purchased from Creative Biolabs (Shirley, NY). Human IgG isotype control was purchased from Thermo scientific (Louise, MO). Bifunctional chelating agent 2-(4-isothiocyanatobenzyl)-1,4,7,10-tetraazacyclododecane-1,4,7,10-tetraacetic acid (*p*-SCN-Bn-DOTA) was obtained from Macrocyclics (Plano, TX). ^{111}In was purchased from Nordion as indium chloride (Kanata, ON). ^{225}Ac (0.05 M HCl) was received from Oak Ridge National Laboratories as an actinium nitrate (Oak Ridge, TN). All chemicals and reagents obtained from Sigma-Aldrich (St. Louise, MO) were used without further purification.

Cell culture

Human breast cancer cell line MCF-7/Her18 that overexpresses IGF-1R was kindly provided by Dr. Hung Mien-Chie (M.D. Anderson Cancer Center, Houston, TX). MCF-7/Her18 cells were maintained in DMEM containing high glucose levels and 10% fetal bovine serum (FBS). Triple negative human breast cancer cell line SUM149PT was purchased from Astrand Bioscience (Detroit, MI). SUM149PT cells were maintained as monolayer in a culture flask containing Ham's

F-12 medium supplemented with 10% FBS (25 mL), hydrocortisone (1 mg/mL, 500 µL), and insulin (10 mg/mL, 250 µL) at cultured at 37˚C in a humidified atmosphere with 5% CO_2. Prior to *in vitro* and *in vivo* use, cells were detached using trypsin-EDTA.

Conjugation and Quality Control of Immunoconjugates

Conjugation of antibodies was performed as reported earlier [22]. The excess unreacted chelator was removed by centrifugation using an Amicon Ultra-10K (Burlington, MA) molecular filtration device. The resulting solution was filtered using a 0.22 µm Millipore filter and stored at -80°C for labeling with ^{111}In and ^{225}Ac. Purity of cixutumumab, DOTA-cixutumumab, control IgG, and DOTA-control IgG was determined using SEC-HPLC (Waters 2796 Bioseparations Module, Waters 2487 Dual λ Absorbance Detector, XBridge® BEH 200A SEC 3.5 µm 7.8 x 300 mm column, Waters Corporation). The UV-Detector was set at 220 and 280 nm and the solvent system was PBS at a flow rate of 0.6 mL/min. Further, the size and purity was characterized by automated electrophoresis (2100 Bioanalyzer system, Agilent).

Bioanalzyer

Binding kinetics between the antibodies and target proteins were measure with ForteBio Octet RED384 (PALL Corporation). Antibodies were immobilized on Anti-human IgG Fc capture sensors (Forte Bio: 18-5060) according to manufactures instructions. Briefly, sensors were incubated in buffer for 120 seconds and then moved to wells containing 100 nM of antibody and incubated for another 180 seconds. After immobilization, sensors were incubated in buffer again for 120 seconds to establish a stable baseline. Antibodies were then exposed to 500 nM, 166 nM, and 55 nM concentrations of Human IGF1R protein (Sino Biological: 10164-H08H) for 120 seconds to obtain the association curve. This was followed by incubation in buffer for another 300

seconds to obtain the dissociation curve. At the same time, empty sensors were exposed to the same concentrations of target protein. This is used during analysis for subtraction of non-specific binding. All reactions were performed with a shake speed of 1000 rpm at 30 °C in 1 × kinetics buffer (Forte Bio: 18-5032). The equilibrium dissociation constant (K_D) was obtained using a 1 to 1 model with global fitting. Data analysis and curve fitting was performed using Data Analysis software 7.1.0.33 (Forte Bio).

Biolayer Interferometry

Binding kinetics between cixutumumab and DOTA-cixutumumab and IGF-1R was measured using biolayer interferometry (BLI) using ForteBio Octet RED384 (PALL Corporation, CA). Antibodies were immobilized on Anti-human FAB-CH1 sensors (18-5104, Forte Bio) according to manufactures instructions. The equilibrium dissociation constant (K_D) was obtained using a 1 to 1 binding model with global fitting. Data analysis and curve fitting was performed using Data Analysis software 7.1.0.33 (Forte Bio).

Flow Cytometry

MCF-7/Her18 cells were treated with antibodies at twelve concentrations ranging from 1000 – 0.015 nM, incubated for 30 min at room temperature, and then cooled on ice for 15 min. Cells were washed with PBS + 2% FBS and incubated with secondary antibody FITC-labeled Goat $F(ab')_2$ fragment anti-human IgG (H + L) (1:50 ratio) (IM0839, Beckman Coulter) for 30 min at 4°C, and then washed again. Flow data was acquired using a Beckman Coulter Gallios flow cytometer (Beckman Coulter) and analyzed by FlowJoV10.6. The EC_{50} was determined using GraphPad Prism 6.

Internalization of Immunoconjugates

MCF7/Her18 cells (10,000 per well) were plated on flat-bottom 96 well plates and incubated 12 h prior to assay by using IncuCyte S3 Live cell imaging system (Essen BioScience, Ann Arbor, MI). Briefly, cixutumumab immunoconjugates or control IgG isotype (4 μg/mL) mixed with IncuCyte FabFluor reagent (Essen BioScience, Ann Arbor, MI) at a molar ratio of 1 to 3 in complete growth media and incubated for 15 min at 37° C. FabFluor labeled antibody (50 μL) was then added directly to cells (in 50 μL). Following addition of Ab/Fab complex, assay plates were immediately placed in an IncuCyte® S3 live-cell imager. Images were captured every 2 hours (from 2 to 48 hours) using a 10× objective lens with phase contrast and fluorescence channel. During each scanning, 5 images were acquired until the end of the experiment. Images were automatically analyzed using the integrated IncuCyte software for phase confluence (measure of cell area) and red fluorescence object area (index FabFluor labeled internalized antibody). Top Hat subtraction was used to minimize any background fluorescence signal.

Radiolabeling and Quality Control of Radioimmunoconjugates

Radiolabeling of DOTA conjugated antibodies with $^{111}InCl_3$ was performed as per the standard lab protocol [22]. After labeling, the reaction was monitored using iTLC strip with 100 mM sodium citrate buffer (pH 5.0) as the mobile phase and analyzed using ScanRam (LabLogic, Brandon, FL). ^{111}In-labeled conjugates were purified using Amicon Ultra-4 centrifugal filters (10K, EMD Millipore, Burlington, MA) with PBS. The purity of the radiolabeled immunoconjugates were determined using size exclusion radio-HPLC and iTLC. A radiochemical purity (RCP) of more than 95% was considered good for *in vitro* and *in vivo* experiments.

For radiolabeling with ^{225}Ac, ^{225}Ac-nitrate (1.0 MBq), previously reconstituted with 0.05 M HCl (Optima grade, Fisher scientific) was added to a 1.5 mL microtube. To this was added L-ascorbic acid (150 g/L; 10 μL), 150 mM ammonium acetate (pH 6.0, 25 μL), and DOTA-cixutumumab (125 μg). The pH of the reaction was determined by spotting 1 μL of the reaction mixture onto Hydrion pH paper (range, 5.0 – 9.0) (Sigma-Aldrich); pH of a typical reaction was 5.8. The reaction mixture was incubated at 37 °C on a shaker at 650 RPM for 2 h. After this, a small aliquot (0.5 μL) was spotted on a iTLC strip to determine the extent of incorporation of ^{225}Ac onto the protein using mobile phase of 50 mM sodium citrate (pH 5.2). Purification of the ^{225}Ac-cixutumumab was done using Amicon Ultra-4 centrifugal filters (10K, EMD Millipore, Burlington, MA) with PBS. The radioactivity was detected using a flow through radioHPLC-detector (Flow-RAM, Broomhill, UK).

The stability of the radioimmunoconjugates was investigated by adding 50 μL of radiotracer to 1.0 mL of plasma or PBS, followed by incubation at 37 °C for up to 7 or 10 days (n = 3). Aliquots of 2 – 5 μL were taken at different time points and analyzed for radiochemical purity using iTLC. The immunoreactive fraction of ^{111}In-cixutumumab was determined as described previously[23, 24].

In Vitro Cytotoxicity

In vitro cytotoxicity (EC_{50} values) of cixutumumab immunoconjugates was determined using IncuCyte S3 Live-cell imager. (Essen BioScience, Ann Arbor, MI). Briefly, 3,000 – 5,000 (SUM149PT) cells were seeded 24 hours prior to treatment in a 96 well plates. The next day, the media was removed and washed with PBS. Cells were then incubated with IncuCyte® Cytotox Red reagent diluted in complete media (1×, Essen Bioscience Cat #4632) for 3 h before treatment. Cells

were treated with different concentrations (500 – 0.2 nM) of cixutumumab, control IgG, ^{225}Ac-cixutumumab and ^{225}Ac-control IgG. The plate was incubated at 37 ˚C for 30 min prior to imaging. Live cell images were captured every 2 hours using a 10× objective lens using phase contrast and fluorescence channel. During each scanning five images were acquired until the end of the experiment. Images were processed and analyzed using IncuCyte S3 software. The red fluorescent values were generated and EC_{50} values for individual compounds were calculated using GraphPad prism 5.03.

Tumor Xenograft, MicroSPECT/CT Imaging and Biodistribution

All animal studies were approved by the University of Saskatchewan Animal Care and Use Committee in accordance with the guidelines set forth in Use of Laboratory Animals (protocol # 20170084). Mice were housed under standard conditions in approved facilities with 12 h light/dark cycles and given food and water ad libitum throughout the duration of the studies. Female nude mice were purchased from the Charles River Laboratory (Sherbrooke, QC). For inoculation, SUM149PT cells (5 x 10^7 cells/mL) were resuspended in a 1:1 mixture of phosphate-buffered saline: Matrigel (BD Biosciences). Each mouse was injected in the right flank with 0.2 mL of the cell suspension. Mice were used for imaging and biodistribution studies when the tumors reached 200 – 400 mm^3.

Mice bearing SUM149PT xenograft received a tail vein injection of 10 ± 0.3 MBq (20.1 ± 0.5 μg; specific activity 0.5 MBq/μg) ^{111}In-cixutumumab, or control ^{111}In-control IgG. At 24, 48, 96, and 120 h post injection, SPECT images were acquired using Vector4CT scanner (MILabs, Utrecht). The imaging and reconstruction parameters, and animal care during imaging was described earlier [22]. For quantification, CT and SPECT images were analyzed using PMOD 3.8

biomedical image analyzing software (PMOD, Switzerland). A 3D region-of-interest (ROI) was manually drawn to encompass the radioactivity uptake in the organ of interest. Tracer uptake was expressed as % IA/mL of tissue volume (% IA/cc). The result was reported as mean ± standard deviation within each study group. After microSPECT imaging, mice were sacrificed at 144 h post injection. Additional groups of mice were administered with the agents and sacrificed at 72 h post injection. The activity was measured using gamma counter and activity in organs was expressed as percentage injected activity per gram organ weight (% IA/g).

^{225}Ac-radioimmunotherapy

When xenografts average size of about 50 mm^3, mice were randomized into 5 groups ($n \leq 8$ per group). We evaluated the effectiveness of two doses of cixutumumab (2.5 mg/kg per dose), ^{225}Ac-cixutumumab (specific activity 8.0 kBq/μg, 225 nCi, 1 μg (~ 0.05 mg/kg) per dose), ^{225}Ac-cixutumumab (specific activity 0.15 kBq/μg, 225 nCi, 51 μg (2.5 mg/kg) per dose), isotype control ^{225}Ac-control IgG (specific activity 0.15 kBq/μg, 225 nCi, 51 μg (2.5 mg/kg) per dose) per dose) following a tail vein injection. Tumor growth was monitored by measuring the greatest length and width using a digital caliper (tumor volume = length × $width^2/2$). The study was terminated when xenograft reached a volume ≥ 1500 mm^3 and this was used to determine survival in the different groups using Kaplan Meier curves. Individual body weight of mouse was recorded during the quarantine (every other day) and experimental period.

Statistical Analysis

All data was expressed as the mean ± SD or SEM of at least 3 independent experiments. Statistical comparisons between the experimental groups were performed by 1-way ANOVA with Bonferoni

multiple comparison post hoc test (multiple-group comparison). Survival was described as median, and survival curves were compared with the log-rank (Mantel-Cox) test. Graphs were prepared and *p* values calculated by using GraphPad Prism (version 5.03; GraphPad, La Jolla, CA). *P* values of less than 0.5 were considered significant.

Results

Conjugation and Quality Control

The conjugation of *p*-SCN-Bn-DOTA to cixutumumab or control IgG resulted in a clear solution with no particulate matter or milky appearance. The purity of DOTA-cixutumumab and DOTA-human-IgG were > 98% on HPLC with < 2% aggregates. Immunoconjugates were further characterized for stability, binding to recombinant IGF-1R, aggregation, and size. Bioanalyzer showed that cixutumumab and DOTA-cixutumumab were > 98% pure with molecular weights of 146.3, and 148.5 kDa, respectively (Fig. 1A). Antibodies were labeled with an average three DOTA molecules per antibody when a chelator to antibody ratio of 16:1 was used in the conjugation reaction. HPLC profiles were identical between conjugated and unconjugated antibodies, showing > 95% purity, which was similar to the bioanalyzer results.

The effect of DOTA conjugation on cixutumumab binding to recombinant IGF-1R was studied using biolayer interferometry. The binding constant (K_D) for cixutumumab and DOTA-cixutumumab was 2.2 ± 0.2nM and 1.6 ± 0.1 nM, respectively (Fig. 1B). Saturation binding of immunoconjugates on MCF-7/Her18 cells was analyzed using flow cytometry. Median Fluorescence Intensity (MFI) was converted into percent bound (Figs. 1C) and plotted against concentration to calculate EC_{50} values of immunoconjugates for MCF7/Her18 cells. The estimated EC_{50} values for cixutumumab and DOTA-cixutumumab were 5.2 ± 1.9 and 21.9 ± 5.9 nM,

respectively (Fig. 1C) and there was no statistical difference between cixutumumab and DOTA-cixutumumab ($p > 0.05$). The control immunoconjugate did not show significant binding affinity to MCF-7/Her18 cells at 100 nM concentration (Fig. S1).

Internalization of Immunoconjugates

A rapid time-dependent increase in red fluorescence was observed with cixutumumab antibodies and not with the isotype control IgG or media control from the first time point (4 h) to endpoint (48 h) of the assay (Fig. 1D). The red signal was observed in the cytosolic compartment of the cells, consistent with the expected localization of the internalized antibody to lysosomes and endosomes. The red object area (μm^2/well) was used to quantify the specific signal. Internalization rate of cixutumumab increased over time with the highest rate being observed at 48 h after incubation (Fig. 1D & Fig. S2).

Radiolabeling and *In vitro* Cytotoxicity

The radiochemical yield of ^{111}In-cixutumumab was 79.5 ± 3.8% at a specific activity of 0.5 MBq/µg. A radiochemical yield of > 95 % was obtained for ^{225}Ac-cixutumumab, with a specific activity of 8.0 kBq/µg. A radiochemical purity of >95% was obtained for ^{111}In-cixutumumab after purification. To investigate the stability of the radioimmunoconjugates ^{111}In-cixutumumab and ^{225}Ac-cixutumumab were analyzed at different time periods by iTLC following storage at 37 ºC in PBS or plasma. In PBS, over 90% of ^{111}In-cixutumumab remained intact after 72 h storage at 37 ºC (Fig. S3A). Additionally, ^{111}In-cixutumumab transchelated in mouse plasma following incubation with 10% of the radiolabel lost at 48 h post incubation (Fig. S3A). ^{225}Ac-cixutumumab

was > 90% intact in PBS after 48 h with similar results seen after incubation in plasma (Fig. S3B). The immunoreactive fraction of ^{111}In-cixutumumab was 77% (Fig. S4).

In vitro cytotoxicity in SUM149PT cells was studied using Incucyte S3 Live cell imager. The EC_{50} of each immunoconjugate was calculated with reference to untreated control cells (Table 1). The EC_{50} of ^{25}Ac-cixutumumab (0.02 nM, 0.5 nCi/mL) in SUM149PT was almost 5000-fold less than the EC_{50} of cixutumumab (95.6 nM). Control IgG had negligible cytotoxicity to these cells with some non-specific cell killing due to ^{225}Ac in the case of ^{225}Ac-control IgG.

MicroSPECT/CT and Biodistribution

MicroSPECT imaging showed persistently high tumor uptake in SUM149PT xenograft (Fig. 2A). ROI analysis at 4 time points is represented as %IA/cc (Fig. 2B). Differences in tumor uptake of ^{111}In-cixutumumab and ^{111}In-control IgG were observed over time (Fig. 2A and B). Uptake of ^{111}In-cixutumumab was visible as early as 24 h p.i. and peaked at around 48 h p.i., before clearing thereafter (9.7 ± 0.4, 9.9 ± 0.5, 6.9 ± 0.8, and 6.2 ± 0.1 %IA/cc at 24, 48, 96, and 120 h p.i., respectively; n = 3). Tumor uptake of ^{111}In-control IgG in SUM149PT was low (4.5 ± 0.9, 4.6 ± 1.1, 3.8 ± 1.4, and 3.6 ± 1.4 %IA/cc at 24, 48, 96, and 120 h p.i., respectively; n = 3). ^{111}In-control IgG tumor uptake was significantly lower than ^{111}In-cixutumumab at all the time points (24 to 120 h; 24 h, $p < 0.001$; 48 h, $p < 0.001$; 96 h, $p < 0.01$; 120 h, $p < 0.05$). Liver uptake of ^{111}In-cixutumumab in SUM149PT tumor-bearing mice displayed (9.3 ± 1.3, 7.3 ± 1.5, 4.1 ± 1.0 and 3.8 ± 0. 9 %IA/cc, n = 3) at 24, 48, 96 and 120 h p.i., respectively (Fig. 2B). Control radioimmunoconjugate had higher uptake in the liver (Fig. 2C) and muscle (Fig. 2D). Highest tumor-to-background was observed at 120 h p.i. for ^{111}In-cixutumumab (11.5 ± 1.1), whereas ^{111}In-control IgG was 3.0 ± 0.5 ($p < 0.001$) (Fig. 2E).

Mice were euthanized at 72 and 144 h p.i. for the biodistribution. Tumors, blood, liver, and spleen of the mice had significant radioactivity accumulation at 72 and 144 h p.i. (Fig. 3A and B) as expected, since radiolabeled antibodies typically have long circulation half-lives and hepatic clearance. Tumor uptake (5.4 ± 0.8 %IA/g) of ^{111}In-cixutumumab at 72 h p.i. was higher ($p < 0.001$, Fig. 3A) from ^{111}In-control IgG.

Efficacy of ^{225}Ac-labeled Radioimmunoconjugates

We evaluated the effectiveness of two doses of cixutumumab, ^{225}Ac-cixutumumab and isotype control ^{225}Ac-control IgG (Fig. 4A). There were no significant differences in the tumor volumes (± SEM) at the start of treatment: cixutumumab 33.2 ± 5.1 mm^3; ^{225}Ac-cixutumumab (8.0 kBq/μg) 49.9 ± 10.5 mm^3; ^{225}Ac-cixutumumab (0.15 kBq/μg) 25.7 ± 7.2 mm^3; ^{225}Ac-control IgG 40.9 ± 8.7 mm^3; and PBS treated 42.7 ± 11.6 mm^3. Following the second dose (day-16) all 7/7 mice in the cixutumumab group had significantly slower tumor growth as shown by 11.3-fold decrease in tumor volume compared with PBS treated group. Complete remission was seen in 2/7 mice in this group which lasted till the end of the study (day-180) (Fig. S5). The initial tumor response was not sustained in 5/7 mice, which reached the humane endpoint (1500 mm^3) between day-58 and day-100. On day-16, 6/6 mice in the high specific activity ^{225}Ac-cixutumumab (8.0 kBq/μg) group showed a 7.6-fold decrease in tumor volume compared with PBS treated mice (Fig. S5). 1/6 mouse had complete remission which lasted till day-180. Relapse was observed in the other mice in this group. Complete remission that lasted till the end of the study was seen in 2/7 mice in the low specific activity group ^{225}Ac-cixutumumab (0.15 kBq/μg) (Fig. S5). Immediately following administration of the second dose (day-16), average tumor volume in this group was 16.3-fold less the PBS treated mice. Some non-specific tumor control (5.1-fold decrease compared with PBS

treated mice) was in mice treated with ^{225}Ac-control IgG treated group (Fig. S5). However, mice in this group quickly reached study endpoint. There was no significant decrease in body weight in all groups and no toxicity related deaths occurred in any treatment group (Fig. S6).

The Kaplan Meier survival curve of the different groups is shown in Fig. 4B. Median survival (days) of mice in the PBS group was significantly lower than ^{225}Ac-cixutumumab 8.0 kBq/μg group ($p < 0.01$, Log-rank (Mantel-Cox) Test) and ^{225}Ac-cixutumumab 0.15 kBq/μg group ($p < 0.001$, Log-rank (Mantel-Cox) Test). The difference between the cixutumumab and ^{225}Ac-cixutumumab 0.15 kBq/μg group survival curves were no statistically significant ($p > 0.05$, Log-rank (Mantel-Cox) Test). The median survival of the PBS group was 52 days, while that of cixutumumab group was 87.0 days. On the other hand, median survival of the ^{225}Ac-cixutumumab 8.0 kBq/μg and ^{225}Ac-cixutumumab 0.15 kBq/μg groups 103.5 and 122.0 days, respectively. The improvement in survival seen using ^{225}Ac-cixutumumab 0.15 kBq/μg was not statistically different from ^{225}Ac-cixutumumab 8.0 kBq/μg.

Discussion

There is overwhelming evidence that enhanced IGF-1R signaling occurs in cells that are intolerant to anti-EGFR and anti-Her2 targeted therapies as well as chemotherapy[25, 26]. The discovery that IGF-1R was implicated in most cancers and resistance to some targeted therapies was greeted with a lot of excitement and many clinical trials of monoclonal antibodies and tyrosine kinase inhibitors (TKIs) against IGF-1R were initiated, including ganitumab, figitumumab, and cixutumumab. However, most of these agents failed to show any benefit in patients[14, 15]. Reasons for the failed trials have been extensively reviewed [15] and include; 1) Mutations in phosphoinositide 3-kinase render cells resistant to targeting of the IGF-1R by constitutively activate Akt; 2) lack of IGF-1R

biomarkers and poor clinical trial design; and 3) Nuclear translocation of the IGF-1R. For example in the recently failed trial of ganitumab in breast cancer (in patients that had become resistant to tamoxifen), the obvious potential biomarker candidate of tumour expression of IGF-1R was not measured at the time of enrolment. The determination of IGF-1R in tumor samples is usually done by immunohistochemistry on biopsy samples. This procedure is invasive and sample collection is not very reproducible. Our approach was therefore to develop a probe for non-invasive imaging of IGF-1R and a ^{225}Ac-labeled agent for targeted radiotherapy of IGF-1R positive tumors. To that end, cixutumumab was conjugated with DOTA, which resulted in a slight decrease in the binding of the immunoconjugate as shown by biolayer interferometry and flow cytometry. The resulting DOTA-cixutumumab was labeled with ^{111}In or ^{225}Ac for microSPECT/CT imaging and alpha particle therapy, respectively. While others have developed immunoSPECT/PET and fluorescent agents against IGF-1R[27-30], there is no report in the literature of a ^{225}Ac-labeled anti-IGF-1R alpha particle therapeutic agent. IGF-1R is an internalizing antigen. Internalization studies showed 6 – 8.5-fold higher internalization of the cixutumumab compared with control antibody. This attribute in addition to the residualizing nature of ^{111}In and ^{225}Ac make radiolabeled derivatives of cixutumumab a good candidate for anti-IGF-1R theranostics.

Some studies showed that the complex of ^{225}Ac with DOTA is stable with less than 5% loss of the radiolabel after 21 days[31]. In our experience, the complex is not very stable and results in a significant loss of the radiometal over time. Up to 20% of ^{225}Ac was lost from the complex over a period of 10 days. This observation was confirmed by a recent study by Thiele *et al* [32] who showed that just 90% of ^{225}Ac-DOTA was intact one day after challenge with serum. Eighteen-membered ring macrocylic H_2macropa forms more inert and stable complex with ^{225}Ac[32]. Stability issues is

likely to have implications on the efficacy and dosimetry/normal tissue toxicity of DOTA-conjugated ^{225}Ac radiopharmaceuticals, particularly the ^{225}Ac-cixutumumab used in this study.

Heskamp *et al.* conjugated anti-IGF-1R antibody (R1507, Roche) with isothiocyanatobenzyl–diethylenetriaminepentaacetic acid (SCN-DTPA) followed by radiolabeling with ^{111}In[30]. Tumor uptake of ^{111}In-R1507 was evaluated in triple negative SUM149 xenograft following administration of different specific activities (corresponding to 1 – 1,000 μg of antibody) of the radioimmunoconjugate. Highest tumor uptake was observed when 1 μg of ^{111}In-R1507 was administered, with tumor uptake decreasing with increasing mass amounts of the administered antibody: 1 μg (38 ± 11 %IA/g) > 3 μg (35 ± 6 %IA/g) > 10 μg (15 ± 4 %IA/g) > 300 μg (9 ± 1 %IA/g). This trend was suggestive of *in vivo* blocking of IGF-1R binding sites of the tumor with increasing antibody mass. On the contrary, other authors have shown that increasing the mass dose of the antibody can lead to increased non-specific blocking, reduced interaction with FcγRs receptors (e.g. in the liver) and hence increased antibody circulation and tumor uptake [33, 34]. In addition, other factors such as tumor size and K_D of the antibody contribute to the absolute tumor uptake. The K_D of R15017 was 0.1 nM while cixutumumab was 2.2 nM. The average tumor weight at the time of imaging in the present study was 410 mg compared with 112 mg in the Heskamp *et al* study. Smaller well vascularized tumors show higher uptake. Tumor uptake following the administration of 20 μg ^{111}In-cixutumumab in our microSPECT imaging studies was lower compared to those of the Heskamp *et al.* study. A comparison of the Heskamp *et al.* study with this should be interpreted with caution since the *in vivo* pharmacology of cixutumumab and R1507 can be significantly different.

We then investigated the anti-tumor effects of the radioimmunoconjugates. We studied the *in vitro* cytotoxicity using IncuCyte S3 live-cell imaging with Cytotox® Red reagent, which allows for real-time quantification of dead cells (Table 1). ^{225}Ac-cixutumumab was almost 5000-fold

(IC_{50} 95.6 nM vs 0.02 nM) more cytotoxic than cixutumumab to SUM149PT breast cancer cells. This IC_{50} (0.5 nCi/mL) was similar to values obtained using other highly potent ^{225}Ac-labeled radioimmunconjugates [35, 36]. We then studied the effectiveness of the unconjugated antibody cixutumumab and ^{225}Ac-cixutumumab at controlling the growth of SUM149PT xenograft. A review of the literature shows that cixutumumab has been used in doses of 2.5 – 60 mg/kg in preclinical and clinical studies[37]. In the present study, we initially opted for the lower dose, to stay within acceptable toxicity profile, given that a maximum tolerated dose study was not performed. Median survival (days) of cixutumumab (2.5 mg/kg) and ^{225}Ac-cixutumumab (8 kBq/μg; 0.05 mg/kg) was 87.0 and 103.5 days, respectively, compared with 52 days for PBS treated. Interestingly, mice administered with low specific activity agent ^{225}Ac-cixutumumab (0.15 kBq/μg; 2.5 mg/kg) survived longer than the other groups with a median survival of 122.0 days. This group also had complete remission in 2/6 mice. It is likely that the lower specific activity agent (higher antibody mass) resulted in higher effective dose of the alpha particle delivered compared with the higher specific activity administration. Many studies have shown that increasing the mass of administered antibody (lower specific activity) results in enhanced circulation half-life and higher tumor-to-background ratios for radiolabeled antibodies[33], especially for antibodies that have significant FCγR receptor interactions (hence higher non-specific tissue accumulation). This, in additional to the antibody mediated cytotoxic/cytostatic effects likely led to improved survival in the low specific activity ^{225}Ac-cixutumumab (0.15 kBq/μg; 2.5 mg/kg) group compared with the higher specific activity group. In several *in vitro* and *in vivo* models cixutumumab has been shown to bind to IGF-1R thereby leading to decrease receptor phosphorylation and receptor degradation as well as induction of antibody-dependent cell-mediated cytotoxicity (ADCC)[37].

Conclusion

^{111}In-cixutumumab specifically accumulated in triple-negative SUM149 xenografts which allowed for the *in vivo* visualization of IGF-1R using immunoSPECT. We also described for the first time an alpha particle labeled anti-IGF-1R antibody ^{225}Ac-cixutumumab. The best therapeutic outcome was seen in lower specific activity ^{225}Ac-cixutumumab (0.15 kBq/μg; 2.5 mg/kg) immunoconjugate. Given the fact that up to 60 mg/kg of cixutumumab has been administered in clinical studies, future *in vivo* studies will focus on the determining the optimal specific activity for radioimmunotherapy studies. This work shows the potential to enhance the efficacy of anti-IGF-1R antibodies by radiolabeling with a high linear energy transfer alpha particle. Enhanced efficacy can be obtained with the use of a more stable chelator for the alpha emitter (^{225}Ac).

Acknowledgement and Funding

This study was funded by a grant from the Sylvia Fedoruk Centre (J2013-128) and the Canadian Breast Cancer Foundation (No. 300030). ^{225}Ac used in this research was supplied by the Isotope Program within the Office of Nuclear Physics in the Department of Energy's Office of Science.

Conflict of Interest

All authors declare they have no conflicts of interest.

Supporting Information

Supporting information of the binding of cixutumumab to cells by flow cytometry (Fig. S1), internalization studies (Fig. S2), stability of ^{111}In/^{225}Ac-cixutumumab in plasma and saline (Fig. S3), immunoreactive fraction determination (Fig. S4), tumor volumes of individual mouse in all

the groups (Fig. S5) and their respective body weight (Fig. S6) is available in supplementary material.

Table 1. EC_{50} values of antibodies immunoconjugates on SUM149PT cells[a]

	EC_{50} (nM)	EC_{50} (nCi/mL)
Cixutumumab	95.6 ± 1.0	NA
^{225}Ac-cixutumumab	0.02 ± 0.004	0.5 ± 0.1
Control IgG	340.1 ± 1.5	NA
^{225}Ac-control IgG	13.8 ± 0.52	16.0 ± 0.6

Values are the mean of triplicates of at least two independent experiments. NA: Not applicable

Figure Legends

Fig. 1A-D. A) Bioanalyzer electropherograms of ladders, cixutumumab, and DOTA-cixutumumab B) Binding of antibodies to recombinant IGF-1R using biolayer interferometry at different concentrations (55, 166 and 500 nM). C) *In vitro* flow cytometry binding assay in IGF-1R positive MCF-7/Her18 breast cancer cells. An 8- point curve allowed for the estimation K_D of cixutumumab and DOTA-cixutumumab. Percentage of bound was estimated from the relative fluorescence intensity and plotted against concentration. A non-linear curve fitting was used to estimate the K_D values. D). Internalization of cixutumumab antibody conjugates in MCF-7/Her18 cells. MCF-7/Her18 cells were treated with either IncuCyte® FabFluor labeled cixutumumab antibody or IgG1 isotype control (4 μg/mL), HD phase and red fluorescence images (10 ×) were captured every 2 h for 48 h. All data shown as a mean of 6 wells ± SEM.

Fig. 2A-E. A) Representative microSPECT/CT fused images of a mouse bearing SUM149PT xenograft after intravenous injection of ^{111}In-cixutumumab and ^{111}In-control IgG. Time-activity curves of B) tumor, C) liver, D) muscle (c) and tumor/muscle ratios. Data are %IA/cc, expressed as mean ± SD.

Fig. 3A & B. Biodistribution of ^{111}In-cixutumumab, and ^{111}In-control IgG in nude mice bearing SUM149PT xenografts at A) 72 h B) 144 h post injection. Data are %IA/g, expressed as mean ± SD.

Fig. 4A & B: Efficacy of two doses (day 0 and 14) of cixutumumab (2.5 mg/kg), ^{225}Ac-cixutumumab (225 nCi, 0.05 mg/kg, 8 kBq/μg), ^{225}Ac-cixutumumab (225 nCi, 2.5 mg/kg, 0.15 kBq/μg), ^{225}Ac-control IgG (225 nCi, 0.15 kBq/μg, 2.5 mg/kg) and PBS treated mice in IGF-1R positive SUM149PT mouse model. A) Tumor growth curves and B) Kaplan–Meier survival curves. Study endpoint occurred when xenograft volume reached 1500 mm^3, or > 20% ulcerated.

References

1. Islami, F.; Torre, L. A.; Drope, J. M.; Ward, E. M.; Jemal, A. Global Cancer in Women: Cancer Control Priorities. *Cancer Epidemiol Biomarkers Prev* **2017,** *26*, (4), 458-470.

2. Foulkes, W. D.; Stefansson, I. M.; Chappuis, P. O.; Begin, L. R.; Goffin, J. R.; Wong, N.; Trudel, M.; Akslen, L. A. Germline BRCA1 mutations and a basal epithelial phenotype in breast cancer. *J Natl Cancer Inst* **2003,** *95*, (19), 1482-5.

3. Lips, E. H.; Mulder, L.; Oonk, A.; van der Kolk, L. E.; Hogervorst, F. B.; Imholz, A. L.; Wesseling, J.; Rodenhuis, S.; Nederlof, P. M. Triple-negative breast cancer: BRCAness

and concordance of clinical features with BRCA1-mutation carriers. *Br J Cancer* **2013,** *108*, (10), 2172-7.

4. Balko, J. M.; Giltnane, J. M.; Wang, K.; Schwarz, L. J.; Young, C. D.; Cook, R. S.; Owens, P.; Sanders, M. E.; Kuba, M. G.; Sanchez, V.; Kurupi, R.; Moore, P. D.; Pinto, J. A.; Doimi, F. D.; Gomez, H.; Horiuchi, D.; Goga, A.; Lehmann, B. D.; Bauer, J. A.; Pietenpol, J. A.; Ross, J. S.; Palmer, G. A.; Yelensky, R.; Cronin, M.; Miller, V. A.; Stephens, P. J.; Arteaga, C. L. Molecular profiling of the residual disease of triple-negative breast cancers after neoadjuvant chemotherapy identifies actionable therapeutic targets. *Cancer Discov* **2014,** *4*, (2), 232-45.

5. Davison, Z.; de Blacquiere, G. E.; Westley, B. R.; May, F. E. Insulin-like growth factor-dependent proliferation and survival of triple-negative breast cancer cells: implications for therapy. *Neoplasia* **2011,** *13*, (6), 504-15.

6. Litzenburger, B. C.; Creighton, C. J.; Tsimelzon, A.; Chan, B. T.; Hilsenbeck, S. G.; Wang, T.; Carboni, J. M.; Gottardis, M. M.; Huang, F.; Chang, J. C.; Lewis, M. T.; Rimawi, M. F.; Lee, A. V. High IGF-IR activity in triple-negative breast cancer cell lines and tumorgrafts correlates with sensitivity to anti-IGF-IR therapy. *Clin Cancer Res* **2011,** *17*, (8), 2314-27.

7. Ayub, A.; Yip, W. K.; Seow, H. F. Dual treatments targeting IGF-1R, PI3K, mTORC or MEK synergize to inhibit cell growth, induce apoptosis, and arrest cell cycle at G1 phase in MDA-MB-231 cell line. *Biomed Pharmacother* **2015,** *75*, 40-50.

8. de Lint, K.; Poell, J. B.; Soueidan, H.; Jastrzebski, K.; Vidal Rodriguez, J.; Lieftink, C.; Wessels, L. F.; Beijersbergen, R. L. Sensitizing Triple-Negative Breast Cancer to PI3K Inhibition by Cotargeting IGF1R. *Mol Cancer Ther* **2016,** *15*, (7), 1545-56.

9. Gualberto, A.; Pollak, M. Emerging role of insulin-like growth factor receptor inhibitors in oncology: early clinical trial results and future directions. *Oncogene* **2009,** *28*, (34), 3009-21.

10. Kineman, R. D.; Del Rio-Moreno, M.; Sarmento-Cabral, A. 40 YEARS of IGF1: Understanding the tissue-specific roles of IGF1/IGF1R in regulating metabolism using the Cre/loxP system. *J Mol Endocrinol* **2018,** *61*, (1), T187-T198.

11. Xue, M.; Cao, X.; Zhong, Y.; Kuang, D.; Liu, X.; Zhao, Z.; Li, H. Insulin-like growth factor-1 receptor (IGF-1R) kinase inhibitors in cancer therapy: advances and perspectives. *Curr Pharm Des* **2012,** *18*, (20), 2901-13.

12. Cao, L.; Yu, Y.; Darko, I.; Currier, D.; Mayeenuddin, L. H.; Wan, X.; Khanna, C.; Helman, L. J. Addiction to elevated insulin-like growth factor I receptor and initial modulation of the AKT pathway define the responsiveness of rhabdomyosarcoma to the targeting antibody. *Cancer Res* **2008,** *68*, (19), 8039-48.

13. Zha, J.; O'Brien, C.; Savage, H.; Huw, L. Y.; Zhong, F.; Berry, L.; Lewis Phillips, G. D.; Luis, E.; Cavet, G.; Hu, X.; Amler, L. C.; Lackner, M. R. Molecular predictors of response to a humanized anti-insulin-like growth factor-I receptor monoclonal antibody in breast and colorectal cancer. *Mol Cancer Ther* **2009,** *8*, (8), 2110-21.

14. Allison, M. Clinical setbacks reduce IGF-1 inhibitors to cocktail mixers. *Nat Biotechnol* **2012,** *30*, (10), 906-7.

15. Baserga, R. The decline and fall of the IGF-I receptor. *J Cell Physiol* **2013,** *228*, (4), 675-9.

16. Kratochwil, C.; Bruchertseifer, F.; Giesel, F. L.; Weis, M.; Verburg, F. A.; Mottaghy, F.; Kopka, K.; Apostolidis, C.; Haberkorn, U.; Morgenstern, A. 225Ac-PSMA-617 for PSMA-Targeted alpha-Radiation Therapy of Metastatic Castration-Resistant Prostate Cancer. *J Nucl Med* **2016,** *57*, (12), 1941-1944.

17. Kratochwil, C.; Giesel, F. L.; Bruchertseifer, F.; Mier, W.; Apostolidis, C.; Boll, R.; Murphy, K.; Haberkorn, U.; Morgenstern, A. (2)(1)(3)Bi-DOTATOC receptor-targeted alpha-radionuclide therapy induces remission in neuroendocrine tumours refractory to beta radiation: a first-in-human experience. *Eur J Nucl Med Mol Imaging* **2014,** *41*, (11), 2106-19.

18. Doi, T.; Shitara, K.; Kojima, T.; Yoshino, T.; Dontabhaktuni, A.; Rebscher, H.; Tang, S.; Cosaert, J.; Ohtsu, A. A phase I study evaluating cixutumumab, a type 1 insulin-like growth factor receptor inhibitor, given every 2 or 3 weeks in Japanese patients with advanced solid tumors. *Cancer Chemother Pharmacol* **2016,** *77*, (6), 1253-62.

19. Argiris, A.; Lee, J. W.; Stevenson, J.; Sulecki, M. G.; Hugec, V.; Choong, N. W.; Saltzman, J. N.; Song, W.; Hansen, R. M.; Evans, T. L.; Ramalingam, S. S.; Schiller, J. H. Phase II randomized trial of carboplatin, paclitaxel, bevacizumab with or without cixutumumab (IMC-A12) in patients with advanced non-squamous, non-small-cell lung cancer: a trial of the ECOG-ACRIN Cancer Research Group (E3508). *Ann Oncol* **2017,** *28*, (12), 3037-3043.

20. Novello, S.; Scagliotti, G.; de Castro, G., Jr.; Kiyik, M.; Kowalyszyn, R.; Deppermann, K. M.; Arriola, E.; Bosquee, L.; Novosiadly, R. D.; Nguyen, T. S.; Forest, A.; Tang, S.;

Kambhampati, S. R. P.; Cosaert, J.; Reck, M. An Open-Label, Multicenter, Randomized, Phase II Study of Cisplatin and Pemetrexed With or Without Cixutumumab (IMC-A12) as a First-Line Therapy in Patients With Advanced Nonsquamous Non-Small Cell Lung Cancer. *J Thorac Oncol* **2017,** *12*, (2), 383-389.

21. https://clinicaltrials.gov. Accessed August 29, 2019

22. Hartimath, S. V.; Alizadeh, E.; Solomon, V. R.; Chekol, R.; Bernhard, W.; Hill, W.; Casaco, A. P.; Barreto, K.; Geyer, C. R.; Fonge, H. Preclinical Evaluation of (111)In-labeled PEGylated Maytansine Nimotuzumab Drug Conjugates in EGFR-positive Cancer Models. *J Nucl Med* **2019**.

23. Lindmo, T.; Boven, E.; Cuttitta, F.; Fedorko, J.; Bunn, P. A., Jr. Determination of the immunoreactive fraction of radiolabeled monoclonal antibodies by linear extrapolation to binding at infinite antigen excess. *Journal of immunological methods* **1984,** *72*, (1), 77-89.

24. Solomon, V. R.; Gonzalez, C.; Alizadeh, E.; Bernhard, W.; Hartimath, S. V.; Barreto, K.; Geyer, C. R.; Fonge, H. (99m)Tc(CO)3(+) labeled domain I/II-specific anti-EGFR (scFv)2 antibody fragment for imaging EGFR expression. *Eur J Med Chem* **2018,** *157*, 437-446.

25. Lu, Y.; Zi, X.; Zhao, Y.; Mascarenhas, D.; Pollak, M. Insulin-like growth factor-I receptor signaling and resistance to trastuzumab (Herceptin). *J Natl Cancer Inst* **2001,** *93*, (24), 1852-7.

26. Nahta, R.; Yuan, L. X.; Zhang, B.; Kobayashi, R.; Esteva, F. J. Insulin-like growth factor-I receptor/human epidermal growth factor receptor 2 heterodimerization contributes to trastuzumab resistance of breast cancer cells. *Cancer Res* **2005,** *65*, (23), 11118-28.

27. Cornelissen, B.; McLarty, K.; Kersemans, V.; Reilly, R. M. The level of insulin growth factor-1 receptor expression is directly correlated with the tumor uptake of (111)In-IGF-1(E3R) in vivo and the clonogenic survival of breast cancer cells exposed in vitro to trastuzumab (Herceptin). *Nucl Med Biol* **2008,** *35*, (6), 645-53.

28. Fleuren, E. D.; Versleijen-Jonkers, Y. M.; van de Luijtgaarden, A. C.; Molkenboer-Kuenen, J. D.; Heskamp, S.; Roeffen, M. H.; van Laarhoven, H. W.; Houghton, P. J.; Oyen, W. J.; Boerman, O. C.; van der Graaf, W. T. Predicting IGF-1R therapy response in bone sarcomas: immuno-SPECT imaging with radiolabeled R1507. *Clin Cancer Res* **2011,** *17*, (24), 7693-703.

29. Zhang, Y.; Cai, W. Molecular imaging of insulin-like growth factor 1 receptor in cancer. *Am J Nucl Med Mol Imaging* **2012,** *2*, (2), 248-259.

30. Heskamp, S.; van Laarhoven, H. W.; Molkenboer-Kuenen, J. D.; Franssen, G. M.; Versleijen-Jonkers, Y. M.; Oyen, W. J.; van der Graaf, W. T.; Boerman, O. C. ImmunoSPECT and immunoPET of IGF-1R expression with the radiolabeled antibody R1507 in a triple-negative breast cancer model. *J Nucl Med* **2010,** *51*, (10), 1565-72.

31. Maguire, W. F.; McDevitt, M. R.; Smith-Jones, P. M.; Scheinberg, D. A. Efficient 1-step radiolabeling of monoclonal antibodies to high specific activity with 225Ac for alpha-particle radioimmunotherapy of cancer. *J Nucl Med* **2014,** *55*, (9), 1492-8.

32. Thiele, N. A.; Brown, V.; Kelly, J. M.; Amor-Coarasa, A.; Jermilova, U.; MacMillan, S. N.; Nikolopoulou, A.; Ponnala, S.; Ramogida, C. F.; Robertson, A. K. H.; Rodriguez-Rodriguez, C.; Schaffer, P.; Williams, C., Jr.; Babich, J. W.; Radchenko, V.; Wilson, J. J.

An Eighteen-Membered Macrocyclic Ligand for Actinium-225 Targeted Alpha Therapy. *Angew Chem Int Ed Engl* **2017,** *56*, (46), 14712-14717.

33. Alsaid, H.; Skedzielewski, T.; Rambo, M. V.; Hunsinger, K.; Hoang, B.; Fieles, W.; Long, E. R.; Tunstead, J.; Vugts, D. J.; Cleveland, M.; Clarke, N.; Matheny, C.; Jucker, B. M. Non invasive imaging assessment of the biodistribution of GSK2849330, an ADCC and CDC optimized anti HER3 mAb, and its role in tumor macrophage recruitment in human tumor-bearing mice. *PLoS One* **2017,** *12*, (4), e0176075.

34. Dijkers, E. C.; Oude Munnink, T. H.; Kosterink, J. G.; Brouwers, A. H.; Jager, P. L.; de Jong, J. R.; van Dongen, G. A.; Schroder, C. P.; Lub-de Hooge, M. N.; de Vries, E. G. Biodistribution of 89Zr-trastuzumab and PET imaging of HER2-positive lesions in patients with metastatic breast cancer. *Clin Pharmacol Ther* **2010,** *87*, (5), 586-92.

35. McDevitt, M. R.; Ma, D.; Lai, L. T.; Simon, J.; Borchardt, P.; Frank, R. K.; Wu, K.; Pellegrini, V.; Curcio, M. J.; Miederer, M.; Bander, N. H.; Scheinberg, D. A. Tumor therapy with targeted atomic nanogenerators. *Science* **2001,** *294*, (5546), 1537-40.

36. Ballangrud, A. M.; Yang, W. H.; Charlton, D. E.; McDevitt, M. R.; Hamacher, K. A.; Panageas, K. S.; Ma, D.; Bander, N. H.; Scheinberg, D. A.; Sgouros, G. Response of LNCaP spheroids after treatment with an alpha-particle emitter (213Bi)-labeled anti-prostate-specific membrane antigen antibody (J591). *Cancer Res* **2001,** *61*, (5), 2008-14.

37. Kalra, N.; Zhang, J.; Yu, Y.; Ho, M.; Merino, M.; Cao, L.; Hassan, R. Efficacy of anti-insulin-like growth factor I receptor monoclonal antibody cixutumumab in mesothelioma is highly correlated with insulin growth factor-I receptor sites/cell. *Int J Cancer* **2012,** *131*, (9), 2143-52.

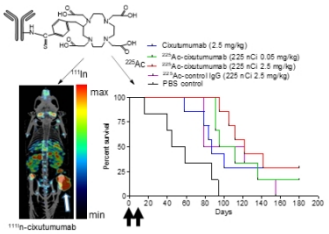

Graphical Abstract

108x60mm (300 x 300 DPI)

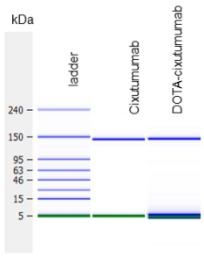

Fig. 1A.

Fig. 1A

108x60mm (300 x 300 DPI)

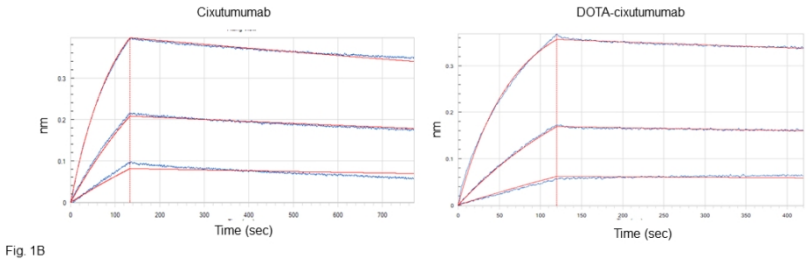

Fig. 1B

Fig. 1B

108x60mm (300 x 300 DPI)

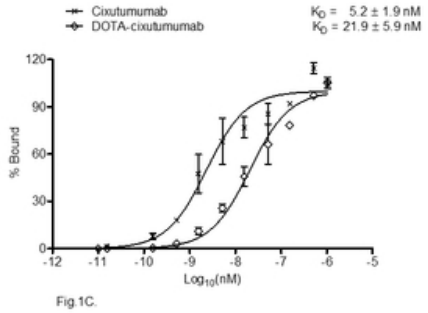

Fig. 1C

27x15mm (600 x 600 DPI)

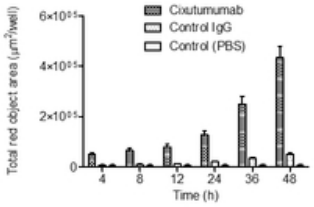

Fig.1D.

Fig. 1D

27x15mm (600 x 600 DPI)

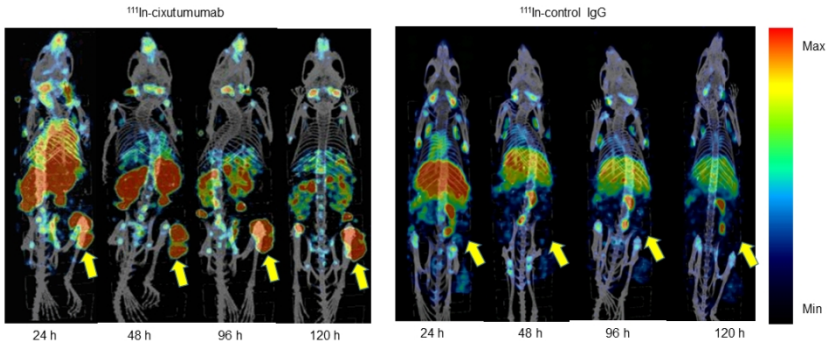

Fig. 2A

Fig. 2A

108x60mm (300 x 300 DPI)

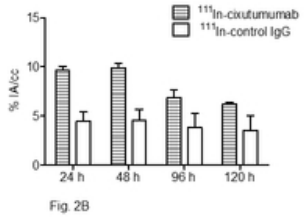

Fig. 2B

27x15mm (600 x 600 DPI)

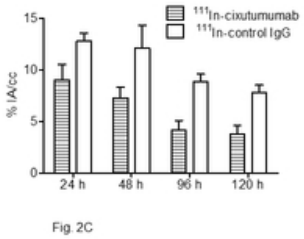

Fig. 2C

Fig. 2C

27x15mm (600 x 600 DPI)

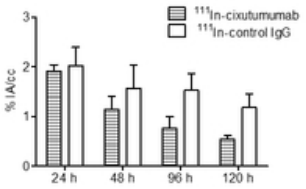

Fig. 2D

Fig. 2D

27x15mm (600 x 600 DPI)

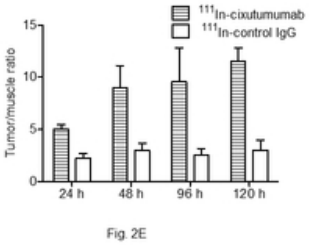

Fig. 2E

Fig. 2E

27x15mm (600 x 600 DPI)

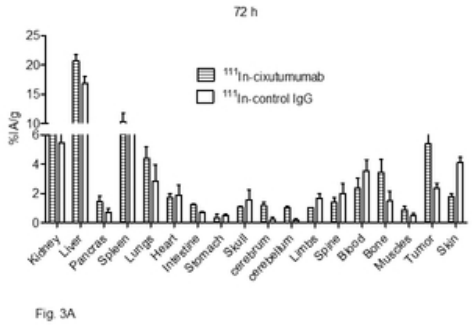

Fig. 3A

27x15mm (600 x 600 DPI)

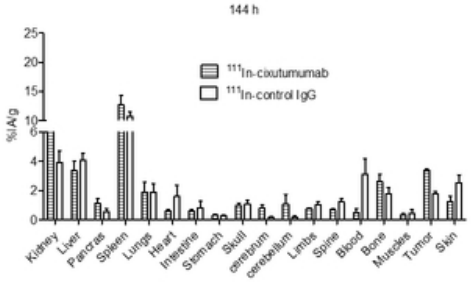

Fig. 3B

Fig. 3B

27x15mm (600 x 600 DPI)

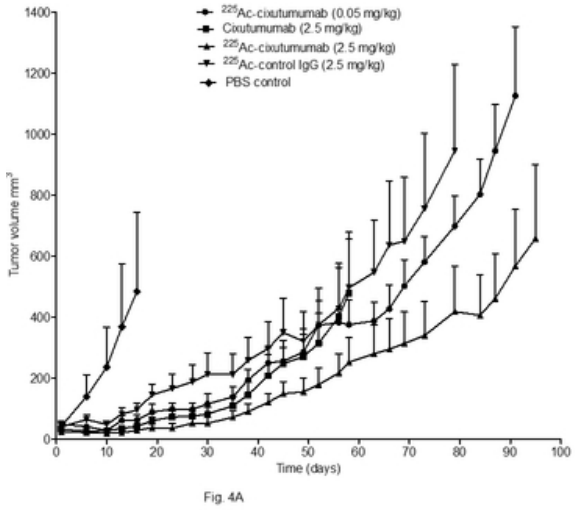

Fig. 4A

Fig. 4A

27x15mm (600 x 600 DPI)

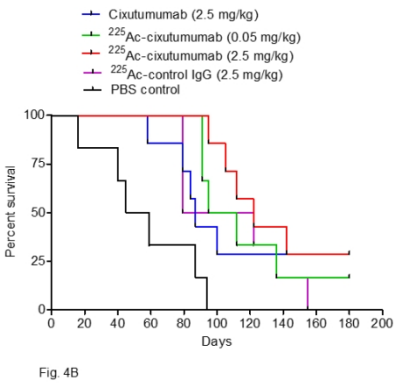

Fig. 4B

Fig. 4B

108x60mm (300 x 300 DPI)